-RESEARCH PAPER-

International Journal of Mining and Geo-Engineering

IJMGE

IJMGE 58-3 (2024) 315-322

DOI: 10.22059/IJMGE.2024.376041.595164

Identifying alterations of Zafarghand porphyry copper system (Isfahan): employing singularity method and false color composite

Seyyed Saeed Ghannadpour [a, *], Morteza Hasiri [a], Hadi Jalili [b] and Hamid Salehi Shahrabi [b]

[a] *Department of Mining Engineering, Amirkabir University of Technology, Tehran, Iran.*

[b] *Iranian Space Research Center, Tehran, Iran.*

Article History:

Received: 02 May 2024.

Revised: 23 June 2024.

Accepted: 14 July 2024.

ABSTRACT

In recent times, geological remote sensing has greatly enhanced the ability to access alteration zones and identify potential sites for hydrothermal deposits quickly and cost-effectively. This study utilizes satellite image processing methods to map the alteration zones in the exploration area of the Zafarghand. The study area is located in the NE of Isfahan and falls within the central structural zone of Iran. The Zafarghand porphyry system exhibits phyllic, potassic, propylitic, and argillic alteration halos. Alterations in this study were detected using ASTER sensor imagery. Each pixel's digital number value from the satellite images, organized in a matrix, serves as a sample in a systematic grid. The singularity method algorithm was then applied as an effective structural tool to identify geochemical anomalies in the digital pixel values from ASTER images. The findings demonstrate that the singularity method, due to its structural attributes, has been successful in decision-making and highly effective on determining promising areas in the study area, especially for propylitic and phyllic alterations.

Keywords: *Singularity, Image Processing, ASTER, Zafarghand, Porphyry Cu.*

1. Introduction

In recent years, Remote Sensing (RS) and geochemical studies have shown their ability to detect deposits in the early stages, especially in their hidden forms. These studies are used in various stages of mineral deposits exploration, especially in the early stages (general exploration stage), and become more critical for deposits that leave relatively large halos compared to the mass of the deposit [1]. Various methods exist for separating and identifying anomalous areas from the background, ranging from non-structural to structural techniques [1]. RS acquires and interprets data about the Earth's surface without direct contact, offering valuable insights for numerous applications, including geological mapping [2-4]. In numerous studies, the application of structural methods for anomaly separation from the background, such as the spatial statistics U method, fractal geometry in various fractal models, and the singularity method, can be observed [1, 5-6]. This study focuses on combining structural techniques for geochemical anomaly detection with standard RS methods to process ASTER satellite images for the Zafarghand exploration zone. The Tethyan Metallogenic Belt, stretching from Eastern Europe to the Middle East, passes through Iran, which encompasses significant segments of this 1700 km belt and hosts major porphyry copper deposits, such as Sarcheshmeh, Miduk, and Dalli. A portion of the belt includes the magmatic arc of Urmia-Dokhtar that the study area is centrally situated within this arc (Figure 1). Early exploration activities in this region comprised geological mapping at a 1:5000 scale, rock sampling, and geophysical surveys [7]. After that, many researches and studies have been done in this area. For example, Sadeghian and Ghafari investigated and studied the petrogenesis of the Zafarghand granitoid mass [8]. Aminoroayaei Yamini et al., with a focus on the mineralogical and geochemical developments of the region, explored the hydrothermal alteration of this deposit [9]. Alaminia et al. conducted geochemical, geophysical, and fluid inclusion studies in 2017 [10]. In another study, Aminoroayaei, described the evaluation of this deposit's magmatic system, considering plagioclase as evidence [11]. Mohammadi et al. examined, through RS studies, the correlation between alteration zones, mineralization, and tectonic structures [12]. In 2016, the porphyry copper of Zafarghand underwent stable isotope and chemical studies to examine the physicochemical parameters of mineralization and related alteration, with a focus on biotite chloritization [13].

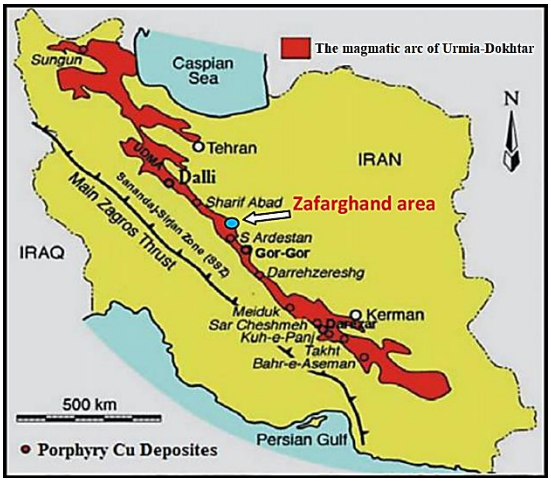

Fig. 1. The study area location in the magmatic arc of Urmia-Dokhtar.

* Corresponding author. *E-mail address:* s.ghannadpour@aut.ac.ir (S. S. Ghannadpour).

Given the significance of this deposit and need for further detailed studies, this research seeks to detect surface geochemical anomalies in the area using ASTER sensor satellite images. The singularity method, known for its effectiveness and efficiency in structural geochemical anomaly separation, will be applied for processing the satellite imagery. In this framework, and particularly in the integration of remote sensing and fractal techniques, many studies have been undertaken. These include the identification of alterations in the exploration areas of Jebal-barez, Tirkan, Takab-Baneh, Tarom, and Saryazd [14-20].

2. The study area

The Zafarghand copper exploration area is situated southeast of Ardestan and 110 km northeast of Isfahan in central Iran. The coordinates for this deposit range from 52°23'55" to 52°26'30" E longitude and 33°10'30" to 33°11'52" N latitude (Figure 2) [10]. The rock units of the region can be seen in Figure 2.

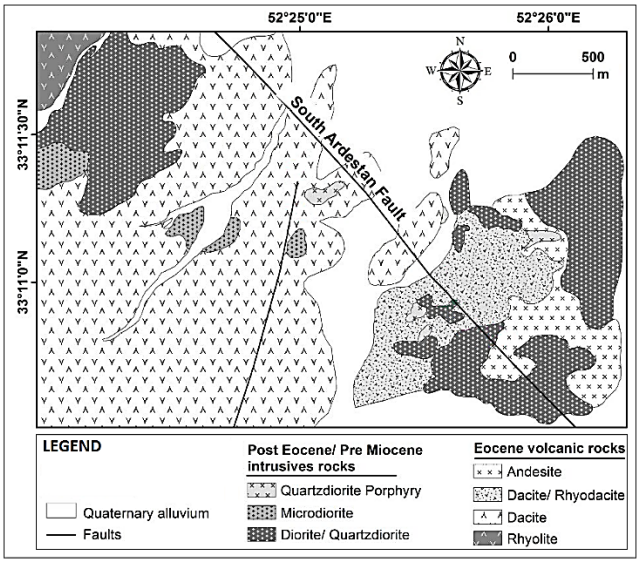

Fig. 2: The geological map of the study area [10].

In the Zafarghand study area, a total of 251 samples were collected to conduct a comprehensive geochemical analysis. These samples include:

Soil Samples (67 samples): These samples were taken from various depths and locations within the study area to assess the geochemical anomalies present in the soil.

Rock Samples (184 samples): The lithological samples collected include various lithologies, such as quartz diorite, diorite, micro diorite, rhyodacite, and dacite.

To facilitate a clearer understanding, the samples in Figure 3 have been differentiated based on their type, providing a visual representation of the distribution and variety of samples collected in the study area. According to the investigation of samples mentioned above and field observation, this area exhibits various types of alteration, including propylitic, argillic, phyllic, and potassic alterations (Figure 3). Some field images of these alterations can be seen in Figure 4 [18].

3. Materials and methods

3.1. Data collection

ASTER satellite images will be applied in this research in order to highlight different alterations. The ASTER sensor with its 14 bands provides valuable information about the Earth's surface. It could be employed with other RS satellites to produce more accurate maps. Combining and comparing the Landsat and ASTER data is the most prominent example of such use [21-22].

3.2. Singularity Method

The singularity method is a method to estimate the concentration of elements using square grids being developed [23]. In order to estimate the concentration with this method, square windows are used to measure the concentration density around a specific position (the target sample) [24]. This method can identify the anomalies hidden in the background, called weak anomalies, which cannot be detected through inverse distance weighting (IDW). In this method, the depletion or enrichment of elements is determined by examining the changes in the concentration of elements with changes in area. The fractal equation of these variables can be calculated from the equation (1) below [25].

$$C(A) = c.A^{(\frac{\alpha}{2}-1)} \quad (1)$$

In this equation, C(A) represents the metal density in area A, c is a constant value, and α is a local singularity value [25]. To determine the value of α, squares with a fixed center in the size of the sides r_i are considered.

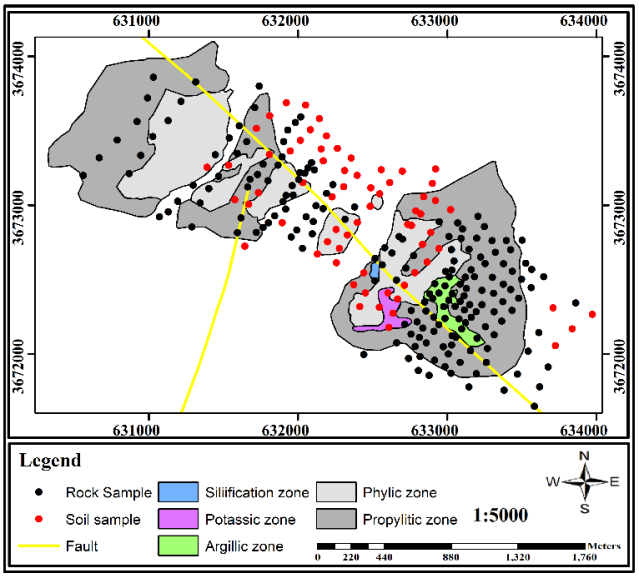

Fig. 3: The extension of alteration halos in the Zafarghand exploration area [10].

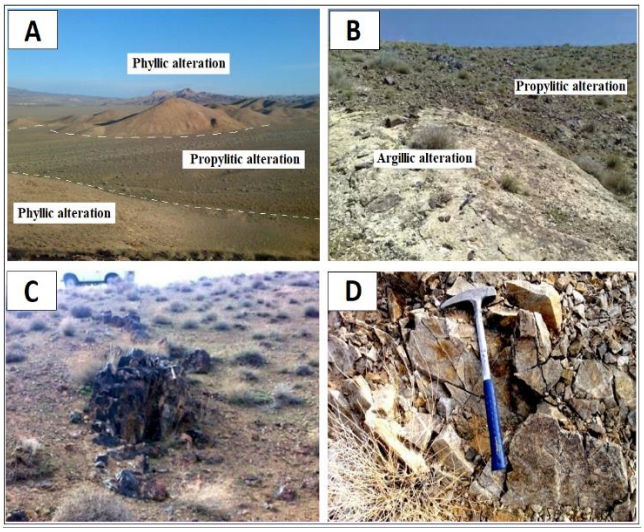

Fig. 4. The field images of alterations in the study area [18]. (a) The outcrop of phyllic and propylitic alteration, (b) The outcrop of argillic and propylitic alteration, (c) Siliceous veins containing copper mineralization in granodiorite rocks with intense potassic alteration (distant view), (d) Diorite rocks with strong potassic alteration (close view).

$$r_i = (2i-1)r_{min} \quad (2)$$

$r_{min} = r_1 < r_2 < \ldots < r_n = r_{max}, \quad i = 1, 2, \ldots, n$

Where n is the number of windows or square grids, r_{min} is the smallest, and r_{max} is the largest window size. It is worth noting that the singularity index is estimated from the slope of the straight line fitted to the pair of data C(A) (average concentration in each window) and r (window size) in a logarithmic plot [26]. In fact, by taking the logarithm of equation (1), the relationship between the window or grid size r_i and the average concentration in each grid (C [A(r_i)]) will be a straight line according to equation (3) [23]:

$$log[A(r_i)] = c + (\alpha - 2)\, log(r_i) \quad (3)$$

Where n is the number of windows or square grids, r_{min} is the smallest, and r_{max} is the largest window size. It is worth noting that the singularity index is estimated from the slope of the straight line fitted to the pair of data C(A) (average concentration in each window) and r (window size) in a logarithmic plot [26]. In fact, by taking the logarithm of equation (1), the relationship between the window or grid size r_i and the average concentration in each grid (C [A(r_i)]) will be a straight line according to equation (3) [23]:

$$log[A(r_i)] = c + (\alpha - 2)\, log(r_i) \quad (4)$$

The value of α-2 can be obtained from the slope of the straight line. The schematic performance of this method is presented in Figure 5.

The operation mentioned above was performed for each position in the study area, and similarly, a singularity value is calculated for each point at the center of the initial square.

The α value or singularity index close to 2 indicates a normal distribution for a geochemical map, while regions with a positive singularity (α > 2) represent depletion, and regions with a negative singularity (α < 2) represent the enrichment of element concentration in the target region [27-30].

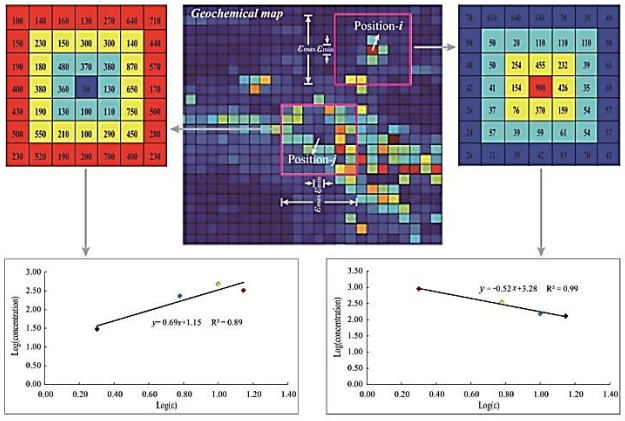

Fig. 5. A schematic representation of the performance of the singularity method [31].

In the following section, at the first step, the pre-processing techniques were applied to the desired images and then, the singularity method was employed for the DN values, taking into their coordinates. Eventually, in order to highlight the desired alterations, band ratio highlighting technique was conducted. Figure 6 shows a visual representation of the study's steps in the form of a flowchart.

4. Processing and results

4.1. Data preparation (preprocessing)

In this section, the preparation and preprocessing of the ASTER satellite image before applying the structural method for anomaly separation from the background are discussed. Before extracting information from satellite images, it is essential to perform radiometric and geometric preprocessing. Preprocessing involves operations that must be conducted first. For georeferencing the image, geometric corrections were employed, while radiometric corrections address issues, including gases, such as oxygen and nitrogen, suspended particles in the atmosphere and sunlight passing through clouds that cause interference.

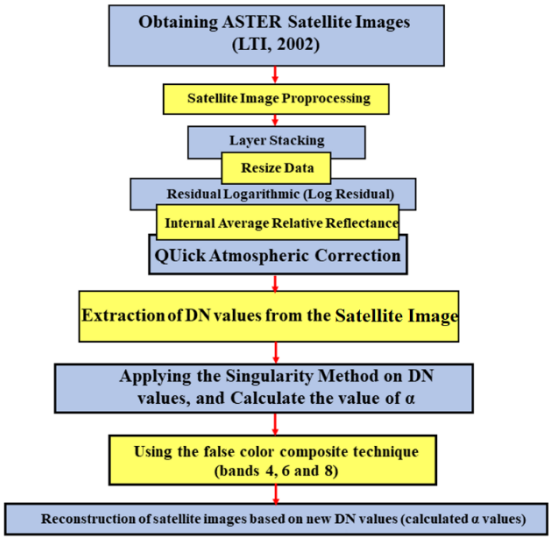

Fig. 6. The flowchart of the steps and process of accomplishing the work.

In this study, according to the nature of considered data (ASTER satellite images), three pre-processing methods, including IARR, Log Residual, and QUAC have been employed [18-20].

4.2. Data extraction from satellite images (ASTER)

After applying the mentioned preprocessing techniques to the ASTER image of the Zafarghand area, the image was prepared for the singularity algorithm. Initially, the ASTER image was cropped (resized) according to the coordinates provided in the geological section, and then, the SWIR range was considered to extract the values of DN (Fig. 7).

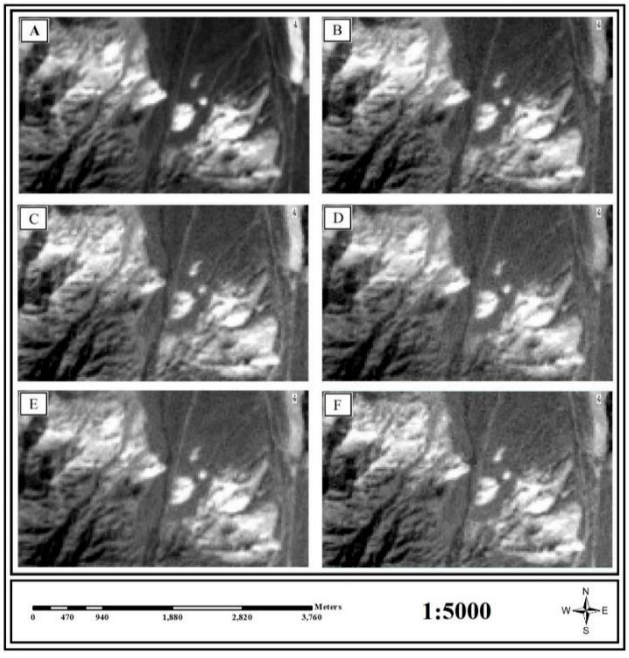

Fig. 7. A resized image of the ASTER sensor (SWIR range). A: Forth band, B: Fifth band, C: Sixth band, D: Seventh band, E: Eighth band, and F: Ninth band.

Table 1 and Figure 8 show the essential statistical characteristics of DN for desired bands and their histograms, respectively. In Figure 8, it can be seen that the values of DN exhibit a normal distribution. Therefore, using anomaly separation methods that typically assume normally distributed data presents no limitations. Following this, the singularity method will be utilized to distinguish anomalous values from the background. The selection of the singularity method, considering the square shape of the image pixels and their average DN value, seems to offer satisfactory performance for this purpose. This effectiveness is due to the raster nature of satellite images, which provide the specific square and its associated digital number (pixel) for the singularity algorithm and allow for the expansion of the required grids (increasing the number of squares).

Table 1. The statistical characteristics of SWIR range bands (bands 4 to 9) corresponding to DN values.

No.	Band	Average	Variance	Standard deviation
1	4	1.7193	0.0988	0.3143
2	5	1.7164	0.0708	0.2660
3	6	1.6378	0.0551	0.2348
4	7	1.4454	0.0256	0.1601
5	8	1.4314	0.0279	0.1671
6	9	1.4126	0.0219	0.1481

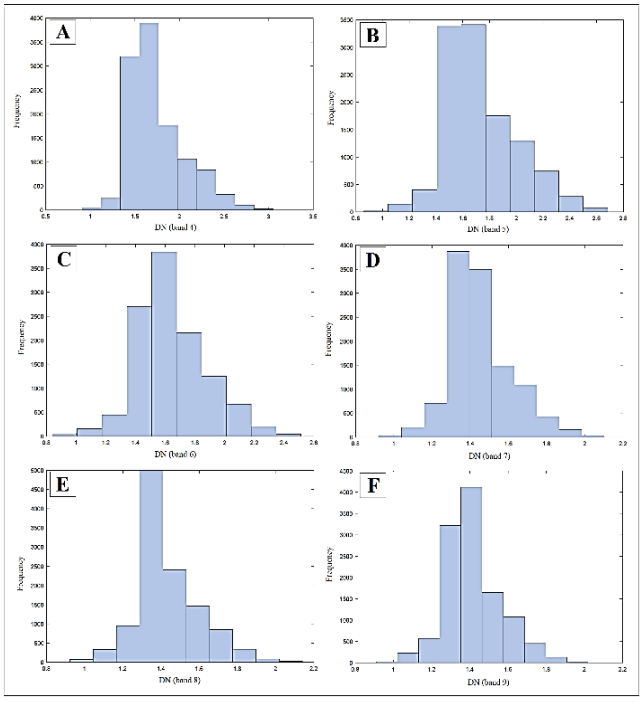

Fig. 8. The frequency diagram of DN value. A: Forth band, B: Fifth band, C: Sixth band, D: Seventh band, E: Eighth band, and F: Ninth band.

5. Applying singularity algorithm on DN values

In this section, to implement the singularity method, the algorithm was first programmed using MATLAB software. The program processes a matrix of values from a systematic grid of data, along with inputs n (the number of windows or square grids) and r_{min} (the size of the smallest square or initial square), providing the singularity index as the output. In the second stage, the values of DN for each band from the SWIR range were input into the singularity method algorithm, with r_{min} set to 30 meters, corresponding to the pixel size of ASTER satellite images in the SWIR range. It is important to note that n was set to 70. Finally, after executing the singularity method algorithm, the α values for the center of each pixel in the image matrix were calculated, and their statistical characteristics were determined (Table 2). The α values histogram is shown in Figure 9.

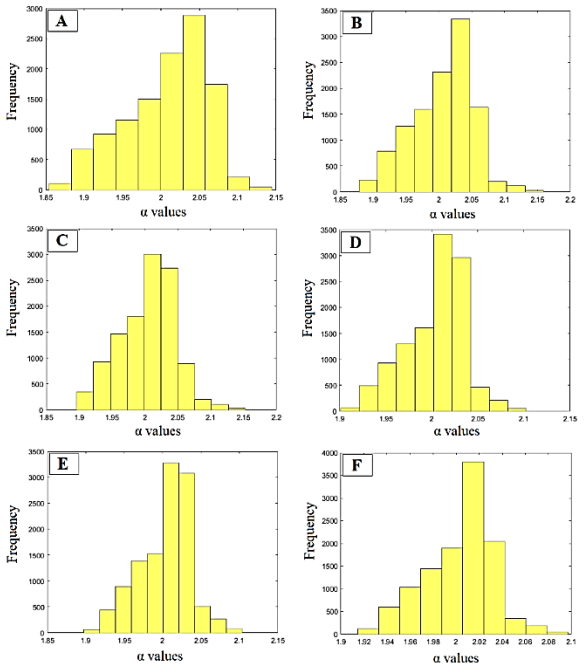

Fig. 9. The frequency diagram of α value for bands. A: Forth band, B: Fifth band, C: Sixth band, D: Seventh band, E: Eighth band, and F: Ninth band.

Table 2. The statistical properties of the α values.

No.	Band	Average	Minimum	Maximum	Variance
1	4	2.0077	1.8543	2.1447	0.0029
2	5	2.0059	1.8786	2.1594	0.0021
3	6	2.0046	1.8962	2.1525	0.0017
4	7	2.0042	1.9013	2.1025	0.0011
5	8	2.0043	1.8973	2.1037	0.0011
6	9	2.0030	1.9144	2.0970	0.0008

Figure 7 indicates that the α values calculated using the singularity method roughly follow a normal distribution. As previously stated, α values less than 2 are considered anomalous, while α values greater than 2 are deemed background values. Consequently, binary images of the Zafarghand area corresponding to the SWIR range bands were generated and are displayed in Figure 10.

In Figure 8, the bright pixels represent α values less than 2 (anomalous values), whereas the dark or black pixels represent α values greater than 2 (background values), as identified by the singularity method applied to ASTER satellite images. However, due to the binary nature and use of black and white colors, these images cannot depict the intermediate intensities of the alterations. Therefore, to more effectively illustrate the performance of this method, the α values themselves were utilized, and the reconstructed image based on α values is shown in Figure 11.

6. False color composite

False color combinations involve merging the red, green, and blue wavelength bands to create images that aid in visual interpretation, especially in identifying geological units. Unlike true color combinations, which reflect the colors of the visible spectrum, false color images result from using various bands of the electromagnetic spectrum, with band selection depending on the specific objective. The human eye is more sensitive to slight color variations in false color images compared to black and white images, which is valuable for identifying geological features. This approach enhances interpretability by simultaneously displaying diverse information from a single point, thereby improving the analysis of geological features [32]. The schematic performance of this technique is presented in Figure 12.

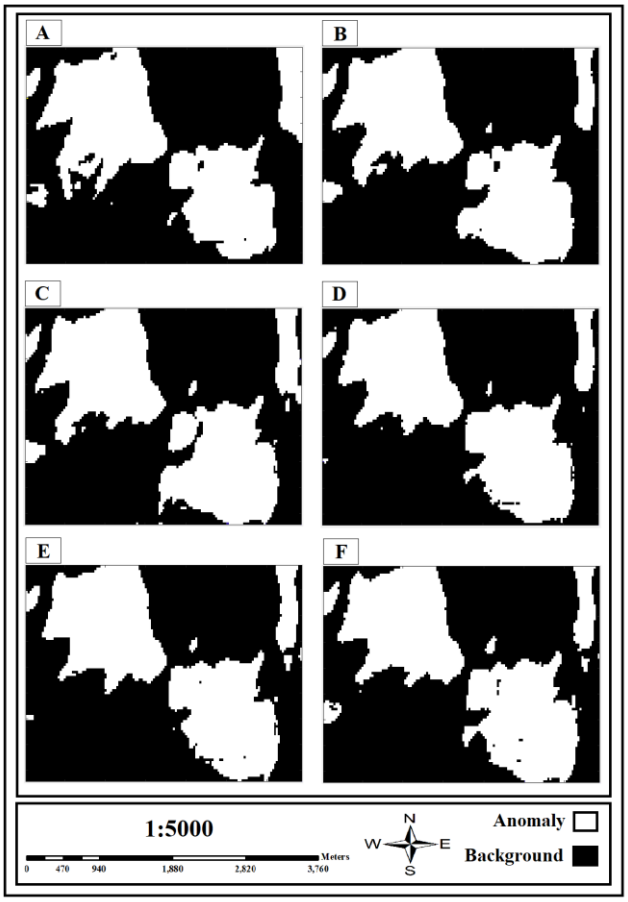

Fig. 10. The binary map of singularity values smaller than 2 (α < 2) of the Zafarghand region, A: Forth band, B: Fifth band, C: Sixth band, D: Seventh band, E: Eighth band, and F: Ninth band.

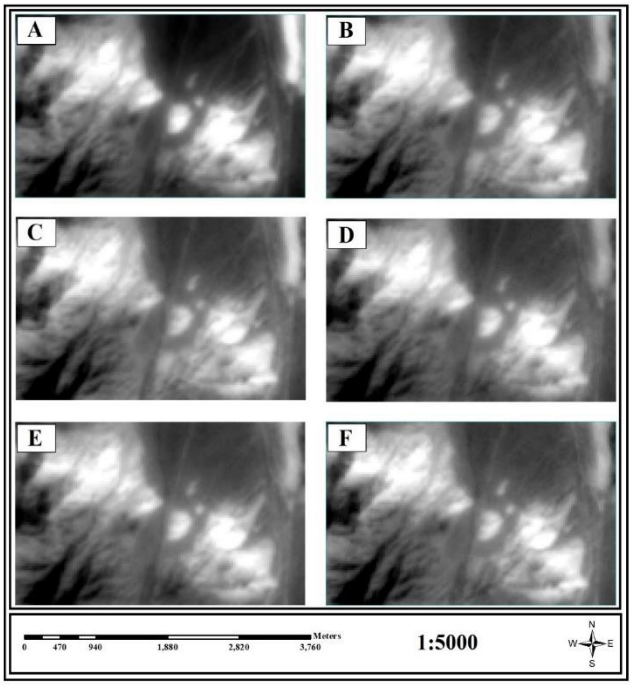

Fig. 11 The reconstructed images of ASTER satellite based on new values of DN (Singularity Index), Forth band (A), Fifth band (B), Sixth band (C), Seventh band (D), Eighth band (E), and Ninth band (F).

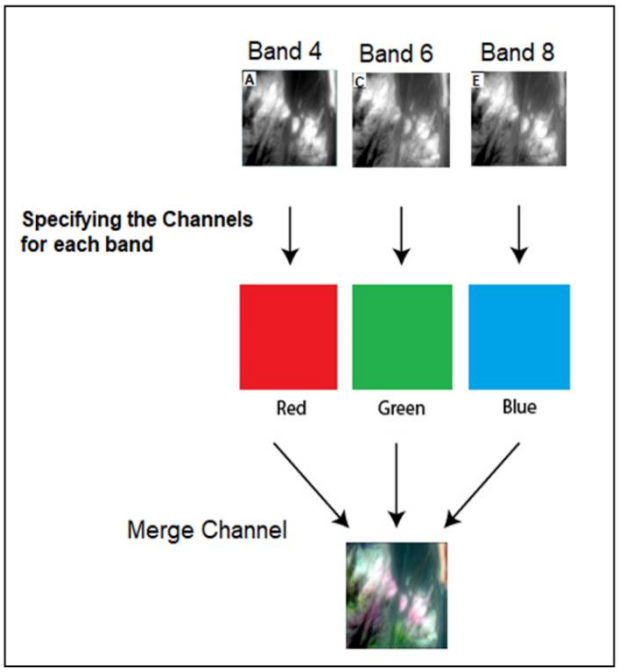

Fig. 12. A schematic representation of the performance of the false color composite technique.

Utilizing color in images enhances the information available conceptually and visually. Experiments have demonstrated that for ASTER images, the RGB=468 composite is an effective composite to detect alterations in most studies, particularly for gold in epithermal and porphyry Cu deposits. Clay minerals, sericite, epidote, and calcite exhibit high reflectivity in ASTER band 4. Epidote and chlorite show significant absorption in eighth band (range 2.33-2.35 μm) due to Fe and Mg-OH [19]. Phyllic alteration is characterized by a pink color, propylitic alteration by a dark green color, and argillic alteration by a red to brown color [21-22]. In this research, a false color image was created using the 4th, 6th, and 8th bands from the reconstructed images based on the α values calculated using the singularity method. The red color was assigned to the reconstructed image of band 4 from the singularity method. Similarly, green and blue colors were assigned to the reconstructed images of bands 6 and 8, respectively. Consequently, the false color image of the Zafarghand exploration area is based on the newly computed values. The DN of each pixel (i.e., α values) is prepared and displayed in Figure 13.

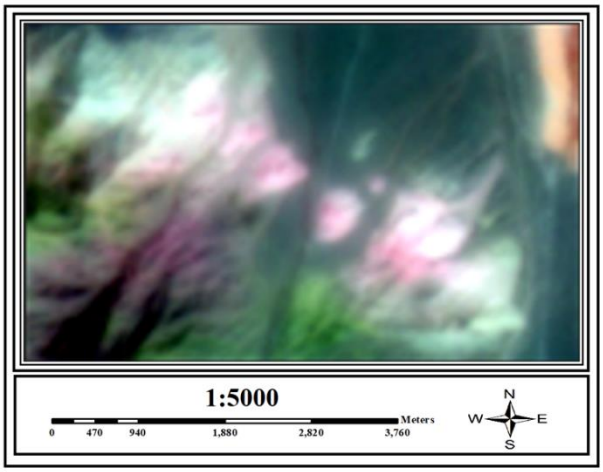

Fig. 13. The false color composite of ASTER Sensor (468) based on singularity index values.

In the resulting image from the false-color composite technique using the α values calculated via the singularity method, green to light green (whitish) represents propylitic alteration, light pink (whitish) signifies phyllic alteration, and pink indicates argillic alteration. As depicted in Fig. 10, the promising zones (anomalous areas) identified by combining the false-color composite and singularity methods closely match the mineralization and alteration zones of the Zafarghand exploration area (Figure 3). More specifically, the light green areas surrounding the light pink halos in the center of the area correspond to propylitic alteration, which overlaps well with the propylitic alterations indicated in Fig. 3. Furthermore, the light pink areas in the center of the image, identified as phyllic alteration, correspond closely with the sericitic alterations shown in Figure 3. To better understand this issue, the final image of propylitic and phyllic alterations (Figure 13) was prepared as an overlay with the alteration map of Figure 3 and can be seen in Figure 14 (parts A and B of Figure 14). Finally, based on the accuracy observed in the results, a final alteration map of the promising areas of the Zafarghand region regarding propylitic and phyllic alterations was prepared and can be observed in Figure 14-C.

The DN values in the northeast and southwest of Figure 13 (or Fig. 14-A and B) indicate phyllic and somewhat propylitic alterations, and their discrepancy with Figure 3 is due to the lack of sampling from these regions. It is worth noting that Fig. 3 is based on surface sampling of the area. Therefore, the absence of sampling from the northeast and southwest regions results in the non-display of alterations in these regions in Figure 3. However, complementary remote sensing studies in the study area have confirmed the presence of such alterations in the northeast and southwest through various satellite image processing methods.

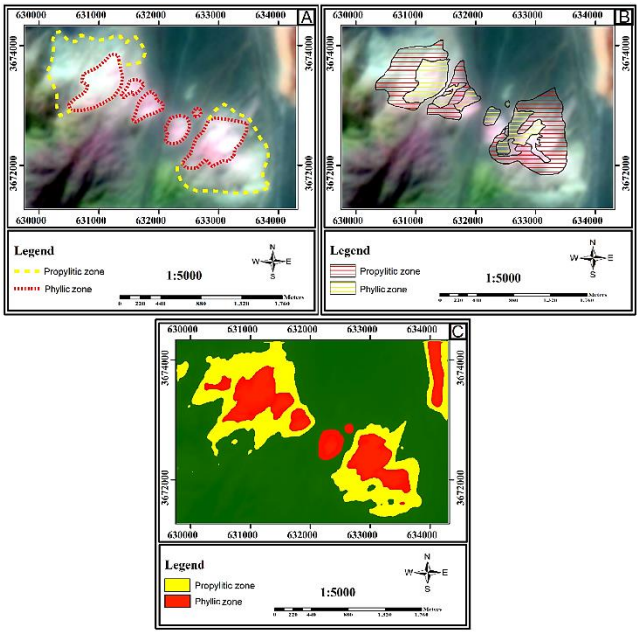

Fig. 14. The final map for alteration zone. A) The identification of phyllic and propylitic alteration zones based on the output of the false color composite method (RGB=468), B) The map resulting from the integration of the false color composite method (RGB=468) and the alteration halos of phyllic and propylitic illustrated in Figure 3, and C) The final alteration map (phyllic, propylitic) in the Zafarghand area derived from new DN values (singularity index) is based on the output of the false color composite method.

Processing remote sensing data, particularly using ASTER, is crucial for translating fluid fluxes associated with hydrothermal mineralization into mappable exploration criteria. ASTER's spectral bands capture DN values indicating Earth's surface radiance or reflectance. Minerals, such as clays, sulfates, carbonates, and hydrothermal products exhibit distinct spectral signatures in the infrared bands (thermal and shortwave). Analyzing these DN values aids geoscientists in mapping mineralogical indicators of fluid flux, integrating data with spectral analysis to produce valuable exploration insights [33-35].

To mitigate uncertainties in targeting mineral prospecting, the most robust approaches and confidence index are integrated within the EIS. Integrating digital number (DN) values from ASTER into the EIS significantly enhances mineral prospectivity mapping by providing detailed spectral data that helps distinguish and determine the features of surface in connection with concentrated fluid flux. The incorporation of ASTER's digital numbers into the EIS, combined with the most robust approaches and indices, significantly improves the accuracy and reliability of targeting mineral prospecting, providing valuable insights into informed decision-making in resource management [36-37].

7. Conclusion

In this study, the singularity method was employed as an effective tool for distinguishing anomalous values from the background. This method is extensively used in various fields of Earth sciences, particularly in exploration geochemistry and economic geology. In this research, the method was applied to process and analyze satellite images to identify and highlight porphyry Cu alterations in the exploration area in NE Isfahan. Satellite images due to their numerical nature (raster images), are stored as matrices of digital number (DN) values for each pixel. Thus, satellite image analysis can be approached similarly to systematic geochemical data. The findings of this study demonstrated that the singularity method, owing to its structural characteristics, is highly effective in separating anomalous values when processing raster-structured satellite images. Consequently, the DN values identified by the singularity method algorithm (α values) show appropriate spatial correlation with each other. Moreover, through the false-color composite technique based on the singularity index, the existing alterations in the images can be effectively identified and highlighted. These alterations are typically associated with specific geological features, such as propylitic and phyllic alterations, which were well identified and confirmed in this study (the final map in Figure 13). These results suggest that using the singularity method in satellite image analysis can significantly enhance the understanding and identification of ground alterations, providing valuable information for mineral exploration and extraction.

Declarations

Ethical Approval

Not applicable to the subject of this research.

Availability of datasets

ASTER satellite image from https://earthexplorer.usgs.gov/ is the sources of the datasets used in the current work.

Conflict of interest

No potential conflict of interest was reported by the authors.

Funding sources

This research did not receive any specific grant from funding agencies in the public, commercial or not-for-profit sectors.

REFERENCES

[1] Hezarkhani, A., & Ghannadpour, S.S. (2015). *Exploration Information Analysis*. Amirkabir University of Technology Publications.

[2] Biranvandpour, A., & Hashim, M. (2014). ASTER, ALI and Hyperion sensors data for lithological mapping and ore minerals exploration. *Springer Plus, 3*, 130.

[3] Ghassemian, H. (2016). A review of remote sensing image fusion methods. *Information Fusion*, *32*, 75–89. Elsevier B.V. doi: https://doi.org/10.1016/j.inffus.2016.03.003

[4] Van der Meer, F., Hecker, C., van Ruitenbeek, F., van der Werff, H., de Wijkerslooth, C., & Wechsler, C. (2014). Geologic remote sensing for geothermal exploration: A review. *International Journal of Applied Earth Observation and Geoinformation*, *33*(1), 255–269. doi: https://doi.org/10.1016/j.jag.2014.05.007

[5] Cheng, Q, Agterberg, F.P., & Bonham-Carter, G.F. (1996). A spatial analysis method for geochemical anomaly separation. *Journal of Geochemical Exploration*, *56*, 183–I95.

[6] Cheng, Q., Yaguang, X., & Eric, G. (2000). Integrated spatial and spectrum method for geochemical anomaly separation. *Natural Resources Research*, *9*(1), 43–52. doi: http://dx.doi.org/10.1023/A:1010109829861.

[7] ANJC (Alamut Naghsh-e Jahan Company). (2011). *Initial exploration report of Zafarghand copper index*, (Isfahan, Iran. 270pp. (in Persian)

[8] Sadeghian, M., & Ghafari, M. (2011). Petrogenesis of the Zafarghand Granitoid Massif (Southeast of Isfahan). *Petrology*, 2(6), 47-70.

[9] Aminoroayaei Yamini, M., Tutti, F., & Ahmadian, J. (2016). Hydrothermal Alteration of Porphyry Copper Deposit in the Southwest of Zafarghand with Emphasis on Mineralogical and Geochemical Changes in the Area. *Journal of Earth Sciences Research*, *7*(25), 75-90. doi: https://dorl.net/dor/20.1001.1.20088299.1395.7.1.6.7.

[10] Alaminia, Z., Bagheri, H., & Salehi, M. (2017). Geochemical and geophysical investigations and fluid inclusion studies in the exploration area of Zafarghand (Northeast Isfahan, Iran). *Journal of Economic Geology*, *9*(2), 29-30. doi: https://doi.org/10.22067/econg.v9i2.56334.

[11] Aminoroayaei Yamini, M., Tutti, F., Amin Al-Raeayaei Yamini, M. R., & Ahmadian, J. (2018). Plagioclase as Evidence of Magmatic Evolution in the Zafarghand Porphyry Copper Deposit, Northeast of Isfahan. *Economic Geology*, *10*(1), 61-76. doi: https://doi.org/10.22067/ECONG.V10I1.49039

[12] Mohammadi, S., Nedaei, A.R., & Aalami Nia, Z. (2018). Analysis of the relationship between mineralization and alteration zones with tectonic structures using remote sensing studies in south Ardestan area (northeastern Isfahan). *Geotectonics*, *7*, 29-47. doi: http://dx.doi.org/10.22077/JT.2020.2434.1013

[13] Aminoroayaei Yamini, M., Tutti, F., Haschke, M., Ahmadian, j., & Murata, M. (2016). Synorogenic copper mineralization during the Alpine–Himalayan orogeny in the Zafarghand copper exploration district, Central Iran: petrogrography, geochemistry and alteration thermometry. *Geological Journal, 25*(2): 263-281.

[14] Fakhari, S., Jafarirad, A., Afzal, P., & Lotfi, M. (2019). Delineation of hydrothermal alteration Zones for porphyry systems utilizing ASTER data in Jebal-Barez area, SE Iran. *Iranian Journal of Earth Sciences*, *11*, 80-92. doi: https://doi.org/10.30495/ijes.2019.664780

[15] Behbahani, B., Harati, H., Afzal, P., & Lotfi, M. (2023). Determination of alteration zones applying fractal modeling and Spectral Feature Fitting (SFF) method in Saryazd porphyry copper system, central Iran. *Bulletin of the Mineral Research and Exploration*, 1-20. doi: http://dx.doi.org/10.19111/bulletinofmre.1264604

[16] Saed, S., Azizi, H., Daneshvar, N., Afzal, P., Whattam, S.A., Mohammad, Y.O. (2022). Hydrothermal alteration mapping using ASTER data, Takab-Baneh area, NW Iran: A key for further exploration of polymetal deposits. Geocarto International 37 (26), 11456-11482

[17] Pourgholam, M.M., Afzal, P., Adib, A., Rahbar, K., Gholinejad, M. (2022). Delineation of Iron alteration zones using spectrum-area fractal model and TOPSIS decision-making method in the Tarom Metallogenic Zone, NW Iran. Journal of Mining and Environment 13 (2), 503-525.

[18] Ghannadpour S.S, Hasiri M, Talebiesfandarani S, Jalili H. (2024) Processing of ASTER satellite images using fractal concentration-area method. Journal of Mineral Resources Engineering: Articles in Press (In Persian with English Abstract).

[19] Ghannadpour S.S, Hasiri M, Jalili H, Talebiesfandarani S. (2024). Satellite Image Processing: Application for Alteration Separation based on U-Statistic Method in Zafarghand Porphyry System (Iran). Journal of Mining and Environment 15 (2), 667-681.

[20] Ghannadpour S.S, Esmailzadeh Kalkhoran S, Jalili H, Behifar, M. (2023). Delineation of mineral potential zone using U-statistic method in processing satellite remote sensing images. International Journal of Mining and Geo-Engineering 57 (4), 445-453.

[21] Esmailzadeh Kalkhoran S, Ghannadpour S.S, Moeini Rad A, Jalili H. (2024). comparing the Performance of ASTER and LANDSAT 8 Satellite Images in Identifying Iron Oxide and Porphyry Copper Alterations in Zafarghand Region of Isfahan Province. Journal of Mineral Resources Engineering 9 (1), 41-65.

[22] Esmailzadeh Kalkhoran S, Ghannadpour S.S, Jalili H, Moeini Rad A. (2024). Investigating porphyry copper alterations and spectral behavior of related minerals using ASTER satellite images in the Zafarghand region, Isfahan. Advanced Applied Geology: Articles in Press (In Persian with English Abstract).

[23] Wang, J., & Zuo, R. (2018). Identification of geochemical anomalies through combined sequential Gaussian simulation and grid-based local singularity analysis. *Computers & Geosciences*, *118*, 52- 64. doi: https://doi.org/10.1016/j.cageo.2018.05.010.

[24] Xiao, F., Chen, J., Hou, W., Wang, Z., Zhou, Y., & Erten, O. (2018). A spatially weighted singularity mapping method applied to identify epithermal Ag and Pb-Zn polymetallic mineralization associated geochemical anomaly in Northwest Zhejiang, China. *Journal of Geochemical Exploration*, *189*, 122- 137. doi: https://doi.org/10.1016/j.gexplo.2017.03.017

[25] Cheng, Q. (2006). GIS-based multifractal anomaly analysis for prediction of mineralization and mineral deposits. In: Harris, J. (Ed.). *GIS Applications in Earth Sciences, Geological Association of Canada Special Paper*, 289–300.

[26] Cheng, Q. (2007). Mapping singularities with stream sediment geochemical data for prediction of undiscovered mineral deposits in Gejiu ,Yunnan Province, China. *Ore Geology Reviews*, *32*(1-2), 314- 324. doi: https://doi.org/10.1016/j.oregeorev.2006.10.002

[27] Liu, Y., Xia, Q., & Carranza, E.J.M. (2019). Integrating sequential indicator simulation and singularity analysis to analyze uncertainty of geochemical anomaly for exploration targeting of tungsten polymetallic mineralization, Nanling belt, South China. *Journal of Geochemical Exploration*, *197*, 143- 158. doi: https://doi.org/10.1016/j.gexplo.2018.11.012

[28] Yilmaz, H., Yousefi, M., Parsa, M., Sonmez, F. N., & Maghsoodi, A. (2019). Singularity mapping of bulk leach extractable gold and −80# stream sediment geochemical data in recognition of gold and base metal mineralization footprints in Biga Peninsula

South, Turkey. *Journal of African Earth Sciences*, *153*, 156–172. doi: https://doi.org/10.1016/j.jafrearsci.2019.02.015

[29] Ghasemzadeh, S., Maghsoudi, A., Yousefi, M., & Kreuzer, O. P. (2023). Spatially weighted singularity mapping in conjunction with random forest algorithm for mineral prospectivity modeling. *International Journal of Mining and Geo-Engineering*, *57*(4), 455–460. doi: https://doi.org/10.22059/IJMGE.2023.366283.595102

[30] Ghasemzadeh, S., Maghsoudi, A., Yousefi, M., & Mihalasky, M. J. (2022). Recognition and incorporation of mineralization-efficient fault systems to produce a strengthened anisotropic geochemical singularity. *Journal of Geochemical Exploration*, *235*. doi: https://doi.org/10.1016/j.gexplo.2022.106967

[31] Xiao, F., Chen, Z., Chen, J., & Zhou, Y. (2016). A batch sliding window method for local singularity mapping and its application for geochemical anomaly identification. *Computers and Geosciences*, *90*, 189–201. https://doi.org/10.1016/j.cageo.2015.11.001

[32] Sharma, R. C., Hara, K., Tateishi, R. (2018). Developing Forest Cover Composites through a Combination of Landsat-8 Optical and Sentinel-1 SAR Data for the Visualization and Extraction of Forested Areas. Journal of Imaging, 4, 105. doi: https://doi.org/10.3390/jimaging4090105

[33] Yousefi, M., & Hronsky, J. M. A. (2023). Translation of the function of hydrothermal mineralization-related focused fluid flux into a mappable exploration criterion for mineral exploration targeting. Applied Geochemistry, 149. doi: https://doi.org/10.1016/j.apgeochem.2023.105561

[34] Parsa, M., Maghsoudi, A., Yousefi, M., & Sadeghi, M. (2016). Recognition of significant multi-element geochemical signatures of porphyry Cu deposits in Noghdouz area, NW Iran. Journal of Geochemical Exploration, 165, 111–124. doi: https://doi.org/10.1016/j.gexplo.2016.03.009

[35] Ja'afar Abubakar, A., Hashim, M., Beiranvand Pour, A., & Shehu, K. (2018). A Review of Geothermal Mapping Techniques Using Remotely Sensed Data. Science World Journal, 12(4), 2017.

[36] Yousefi, M., Carranza, E. J. M., Kreuzer, O. P., Nykänen, V., Hronsky, J. M. A., & Mihalasky, M. J. (2021). Data analysis methods for prospectivity modelling as applied to mineral exploration targeting: State-of-the-art and outlook. Journal of Geochemical Exploration, 229. doi: https://doi.org/10.1016/j.gexplo.2021.106839

[37] Yousefi, M., Kreuzer, O. P., Nykänen, V., & Hronsky, J. M. A. (2019). Exploration information systems – A proposal for the future use of GIS in mineral exploration targeting. In Ore Geology Reviews (Vol. 111). Elsevier B.V. doi: https://doi.org/10.1016/j.oregeorev.2019.103005